Article

Modelling Irradiation Effects in Metallic Materials using the Crystal Plasticity Theory

Karol Frydrych [1,2] (ID)

1 NOMATEN Centre of Excellence, National Centre for Nuclear Research, Sołtana 7, 05-400 Otwock, Poland; karol.frydrych@ncbj.gov.pl

2 Institute of Fundamental Technological Research (IPPT), Polish Academy of Sciences, Pawińskiego 5B, 02-106 Warsaw, Poland

* Correspondence: karol.frydrych@ncbj.gov.pl

Abstract: The review starts by highlighting the significance of nuclear power plants in contemporary world, especially its indispensable role in the global efforts to reduce CO_2 emissions. Then, it describes the impact of irradiation on microstructure and mechanical properties of reactor structural materials. The main part provides the reader with a thorough overview of crystal plasticity models developed to address the irradiation effects so far. All three groups of most important materials are included. Namely, the Zr alloys used for fuel cladding, austenitic stainless steels used for reactor internals and ferritic steels used for reactor pressure vessel. Other materials, especially those considered for construction of future fission and fusion nuclear power plants, are also mentioned. The review pays also special attention to ion implantation and instrumented nanoindentation which are a common way to substitute costly and time-consuming neutron irradiation campaigns.

Keywords: irradiation; crystal plasticity; indentation; ion implantation; neutron; metallic materials; nuclear reactor; structural materials

1. Introduction

The climate scientists report extremely fast gobal warming as a result of enormous CO_2 emissions. The rate of this changes seems to be too fast to be manageable by most of flora and fauna species, as well as modern human civilizations. Therefore, it is important to introduce emission-free energy sources [1]. Although the solar and wind power plants are paid much attention to, they cannot play the dominant role yet, as they are not sufficiently stable and the large-scale storage of electrical energy is still an unsolved problem. Moreover, they require extremely large usage of land in order to fulfil country-scale energy needs and the rate of installing new power plants is not satisfactory. That's why at least some part of energy should come from the nuclear power plants (NPPs) if the CO_2 emissions are to be reduced quickly. It should be also mentioned that apart from being emission-free, the NPPs offer further advantages, such as:

- extremely low amount of fuel (as compared to fossil fuel power plants), which offers the possibility to store the fuel for many years of operation in advance, thus being independent from unstable political situations across the world,
- extremely low amount of waste (as compared to fossil fuel power plants),
- stable electrical energy generation (also heat generation if cogeneration is considered),
- extremely low usage of land (especially as compared to solar, wind and water power plants).

The important materials used in currently operating NPPs are[1]:

---

1 The pressurized water reactors (PWRs, cf. [2]) are considered here, as they are the most commonly operated NPPs.

- zirconium alloys having hexagonal close packed (HCP) lattice. They are used for fuel cladding and thus are subjected to highest radiation. On the other hand, they have to survive only during the time between subsequent fuel replacements (typically around 6 years),
- austenitic stainless steels (ASS) having face centered cubic (FCC) lattice. They are used for reactor vessel internals, which fullfill many functions such as supporting the core, control rod assemblies, core support structure and reactor pressure vessel (RPV) surveilance capsules [3]. As they are inside the RPV, they are subjected to considerable neutron fluxes,
- ferritic steels of body centered cubic (BCC) lattice, such as e. g. US A508C1 or A533B, French 16MnD5, Russian 15Cr2MoVA and Chinese A508-3 steels, are used to build reactor pressure vessel. As the vessel is typically very large and has very thick walls, it is in principle the only part that cannot be replaced. Thus, its lifetime determines the service lifetime of the whole NPP.

As will be seen in the following, most models developed so far dealt with materials belonging to one of those three groups. The studies are driven by practical considerations as e. g. answering the question of RPV life extension [4]. The assessment of irradiation-induced effects on mechanical properties of construction materials in NPPs is crucial as it is strongly related to safety of the unit. Although the irradiation typically leads to increasing the yield strength of the material, it often results also in post-yield softening, decrease of ductility and increase in ductile to brittle transition temperature (DBTT). Other important phenomena are swelling and irradiation growth of the fuel cladding. Therefore, reliable, physically sound and experimentally consistent material models should be built in order to address those issues.

Although the presently built generation III/III+ NPPs are much improved as compared to previous projects, the generation IV (Gen-IV) initiative calls for new nuclear energy systems that will significantly improve [5]:

- safety and reliability,
- sustainability,
- useful reactor life,
- proliferation-resistance,
- profitability.

Generation-IV International Forum (GIF) members identified six systems [6]: very high temperature gas-cooled reactor (VHTR), gas-cooled fast reactor (GFR), sodium-cooled fast reactor (SFR), lead-cooled fast reactor (LFR), molten salt reactor (MSR) and super-critical water-cooled reactor (SCWR). However, the Gen-IV projects typically pose new material challenges. Depending on the particular reactor type, the construction materials should typically sustain (as compared to existing NPPs):

- longer operation times,
- higher radiation doses,
- higher operating temperatures (especially in the case of VHTR),
- more chemically aggressive environments.

Moreover, in the case of future fusion reactors, even higher radiation and temperature are expected.

Therefore, for future generation IV NPPs, in general different materials should be used as outlined in [5,7]. Among the class of metallic materials, four types of steels, namely ferritic-martensitic (FM), austenitic stainless and oxide dispersion strenghtened (ODS) steels (cf. [8]) are enlisted as promising candidates. The ODS steels with FM matrix were designated as those that enable achieving high radiation doses and high burn-ups required in fast reactors. The nickel-based alloys make also an important class of materials, especially in the case of very high temperature reactors. Specifically, none of the steels are considered as suitable for VHTRs, except the ferritic-martensitic steels which are considered as a secondary option. In the case of future fusion power plants, especially harsh conditions
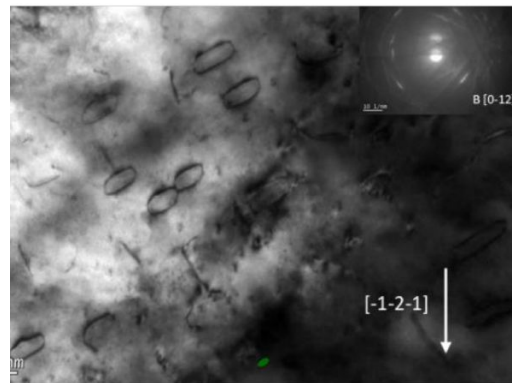
Figure 1. Dislocation loops in irradiated pure iron visible in TEM micrograph [25].

are expected in the case of plasma-facing components. Tungsten has high melting point, low rate of tritium retention, low rate of sputtering and good thermal conductivity [9]. Therefore, tungsten-based materials, e. g. the tungsten-based high entropy alloys [10,11] are considered for this particular application.

2. Irradiation-induced effects

Irradiation leads to changes in the microstructure [12–17] and mechanical properties [18] of materials. The basic mechanism responsible for those changes is the following, cf. e. g. [19,20] and references therein. The energetic particle (neutron in the case of nuclear reactor, ion in the case of ion implantation experiment) collides with the atom present in the crystalline structure of a given metallic material. This collision results in displacing the so called primary knock-on atom (PKA). This atom then interacts with other atoms leading to the cascade of defects occurring in the material. Vacancy-interstitial pairs are thus created. They can then reconfigure leading to creation of defects such as stacking fault tetrahedra (SFT) in FCC lattice or dislocation loops (DLs) in BCC lattice (cf. Fig. 1). The problem is even more complicated in HCP Zr alloys where interstitial-type DLs are formed on the prismatic planes and vacancy-type DLs on the basal ones [21]. Huge amount of irradiation-induced vacancies leads to the formation of voids in the material which can be macroscopically identified as swelling. Other defects, such as precipitates or solute rich clusters (SRCs) [22], can be also created. In the case of RPV steels, the nucleation and growth of Cu, Ni and Mn precipitates due to irradiation is an important issue [23]. According to the dispersed barrier hardening (DBH) model [24], the defects impede the movement of dislocations thus leading to *irradiation hardening*.

Common feature of irradiated materials is also the appearance of defect-free channels (cf. Fig. 2) accompanied by macroscopically observed post-yield softening and ductility loss (cf. Fig. 3, see also [26]). There seems to be a scientific consensus that the channels originate from local annihilation of the irradiation-induced defects by gliding dislocations. This drives the localization and softening. In the course of further deformation, the nucleation, growth and coalescence of voids occurs at the intersection of soft channels with hard material. This can finally lead to fracture. Apart from the neutron-PKA interaction, other mechanisms are possible. For example the nuclear reaction of a given atom with incoming neutron can lead to its transmutation. The Al-Si transmutation in Al-6061 alloy leads to the formation of Si precipitates [27]. Other effect is the generation of He through the (n,α) nuclear reaction. Huge amounts of generated He can lead to formation of He bubbles, cf. Fig. 4.

The amount of neutrons of a given energy flowing through the material can be characterised by their *fluence* Φ, which is equal to the number of neutrons dN penetrating the sphere having the cross section da:
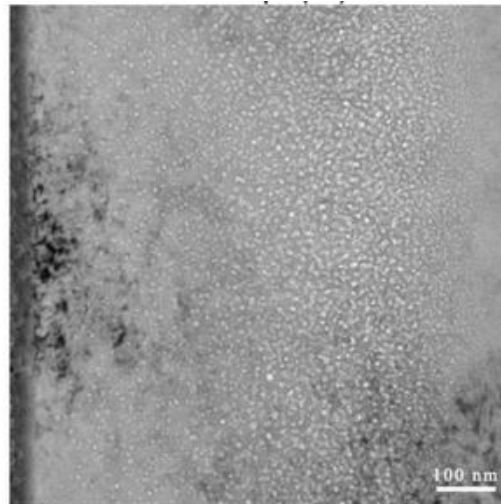
$$\Phi = \frac{dN}{da}.$$
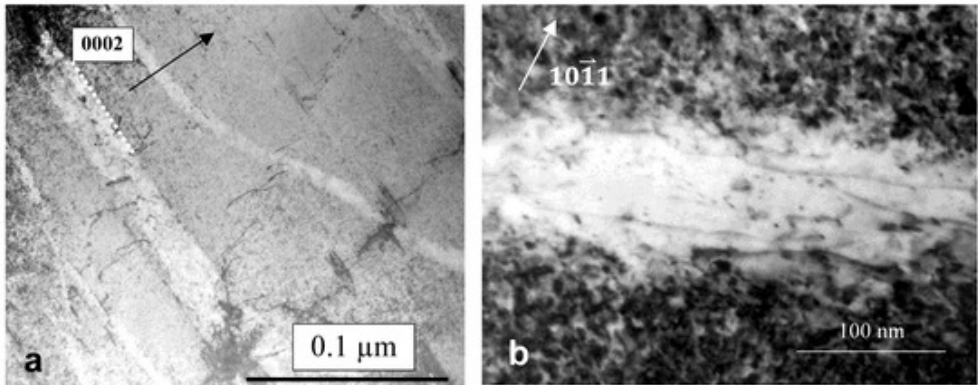
Figure 2. a) Dislocation channels in irradiated and tension-deformed Zircaloy-2, b) dislocations and dislocation loops within the channel [28].
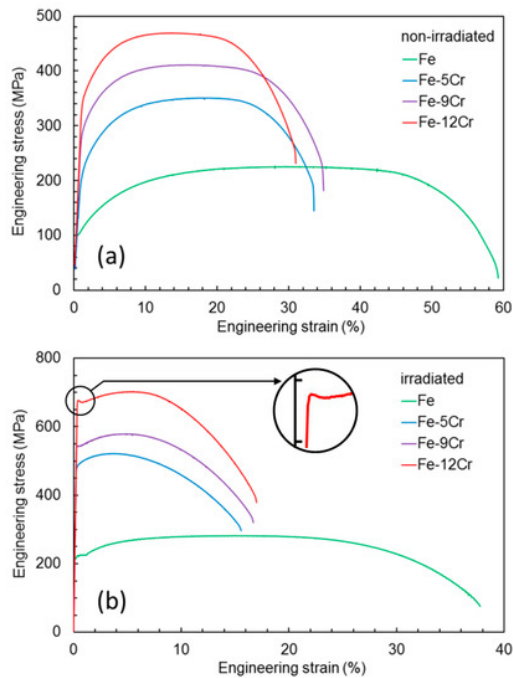
Figure 3. Engineering stress strain curves in iron and iron-chromium alloys in a) virgin and b) irradiated state [29]. Post-yield softening and ductility loss are clearly observed in the irradiated case.

Figure 4. He bubbles in FeCrNi alloy subjected to He implantation seen as bright regions in TEM micrograph [30].

However, from the point of view of mechanics and materials science, the displacement per atom (dpa) [31] provides a better measure of the effects of irradiation on material, as it does not depend on the energetic spectrum of neutrons [32] and can be also applied to ions. In order to calculate dpa in the case of ion irradiation, the SRIM software [33] is commonly used. Recently, the Iradina code [34] was developed. According to its developers, it offers some advantages over the SRIM software.

3. Modelling irradiation effects

There were so far many efforts to take into account the influence of irradiation defects on the mechanical properties of metals and alloys in macroscopic phenomenological models, cf. e. g. [35–40]. However, as could be seen from the previous paragraphs, the phenomena related to radiation-induced microstructure changes appear at different time and length scales and therefore the multiscale modelling approach is the most appropriate in addressing them [18,23]. The fundamental mechanisms and their energetics can be obtained from atomic scale methods, such as molecular dynamics or even ab initio. Larger volumes and longer times can be achieved using coarse grained methods such as kinetic Monte Carlo or dislocation dynamics, utilizing the information gained from atomistic modelling. The next scale is the meso scale that forms a bridge between the discrete and continuum models. Apart from phase field and cluster dynamics, such an approach is the crystal plasticity theory, which is the topic of this review. Readers interested in links between atomistic simulations and constitutive models of irradiated materials are referred to the review [18].

CP predictions can be both directly utilized to obtain the macroscopic response of the specimen, as well as used to get insight into grain-scale phenomena. In general, the crystal plasticity can be crudely divided into so-called phenomenological crystal plasticity (PCP) and dislocation density based crystal plasticity (DDCP) theories. In PCP, the critical resolved shear stress (CRSS) evolves with the amount of accumulated slip, while in DDCP it is related to the evolving dislocation densities. In the PCP model of Deo et al. [41], the CRSS is increased according to the formula (cf. [36]):

$$\tau = \tau_0 + \alpha \mu b \sqrt{Nd}, \tag{1}$$

where τ is the initial CRSS, τ_0 is the unirradiated CRSS, α is the defect cluster barrier strength, μ is the shear modulus, b is the Burgers vector length, N is the defect cluster density and d is their diameter.

In the paper of Onimus and Béchade [42] the crystal plasticity theory was applied to model the behaviour of irradiated zirconium alloy of HCP crystallographic structure. The irradiation hardening was incorporated by modifying the CRSS, similarly as in [41]. However, the population of dislocation loops evolved with accumulated slip. In addition, the fact that the interaction between dislocation loops and mobile dislocations is different for different slip system families was taken into account. Dislocation channelling was also considered. Irradiated ziracalloy was also analyzed in [43]. The irradiation effect was introduced in a similar fashion to the previous papers. The softening effect was taken into account by decreasing the CRSS of basal and prismatic slip after reaching the critical value of slip. Using the model combined with FEM homogenization, it was possible to simulate strain localization, softening and associated ratcheting in irradiated zircalloy subjected to cyclic loading. Thermal creep, irradiation creep and irradiation induced growth were taken into account in the constitutive model reported in [44]. Two micro-macro transition schemes enabling to obtain the response of the polycrystal from single crystal consistitive model were compared, namely the self-consistent method and FFT solver AMITEX_FFTP.

The DDCP model was used to simulate the behaviour of 22NiMoCr37 RPV steel in [45]. Classically, the CP formulations use the power law ([46], see also [47–50]) of the type:

$$\dot{\gamma}^{\alpha} = \dot{\gamma}_0 \left| \frac{\tau^{\alpha}}{s^{\alpha}} \right|^{1/m} \mathrm{sign}(\tau^{\alpha}), \qquad (2)$$

where $\dot{\gamma}^{\alpha}$ is the slip rate on system α, $\dot{\gamma}_0$ is the reference slip rate, s^{α} is the crtical resolved shear stress, m is the rate sensitivity and τ^{α} is the resolved shear stress (RSS). However, since this simplified description is not able to capture the real strain-rate and temperature sensitivity of plastic flow [51], and does not account for the inherent lattice resistance in BCC metals [36], in [45] (and many DDCP models to be described in the following) the thermal activation Kocks-type plastic flow law [52] similar to the one presented in [51] was applied:

$$\dot{\gamma}^{\alpha} = \dot{\gamma}_0 \exp\left(-\frac{\Delta G_0}{k_B \theta} \left(1 - \left(\frac{\tau^{\alpha}_{eff}}{s^{\alpha}_{\star}} \right)^p \right)^q \right), \qquad (3)$$

where $\dot{\gamma}_0$ can be calculated based on dislocation theory [53] or selected as a material parameter, ΔG_0 is the activation free energy required to overcome the obstacles to slip without the aid of an applied shear stress, k_B is the Boltzmann's constant, p and q are exponents that should lie in the range (0,1) and (1,2), respectively. According to [51], $\tau^{\alpha}_{eff} = |\tau^{\alpha}| - s^{\alpha}_a$, and s^{α}_a denotes the part of the resistance due to athermal obstacles to slip (those that cannot be overcome with the aid of thermal fluctuations, such as dislocation groups and large incoherent particles). $s^{\alpha}_{\star}$ represents the part due to thermal obstacles (those that can be overcome with the aid of thermal fluctuations, such as the Peierls resistance, solute atoms and forest dislocations). The evolution of dislocation densities on each slip system was tracked using two terms, namely the storage dependent on mean free path and the annihilation distance. The irradiation was introduced by modifying the initial value of CRSS without explicitly accounting for irradiation-induced defects. However, the paper presented quite detailed analysis of the simulation results as concerns the probabilistic assessment of brittle fracture.

Krishna et al. [19] developed the crystal plasticity model for FCC copper. The model seems to be the first one tracking both the evolution of dislocation and defect densities. Dislocation populations on each slip system were taken into account. Also the defects (SFTs) for each slip system were accounted for. Such an approach allowed to successfully capture the increase in yield stress followed by yield drop and non-zero stress offset from the unirradiated stress-strain curve. Capturing these phenomena was possible due to the interplay of the dislocation density evolution (two terms – growth and dynamic recovery)

and defect annihilation due to the interaction with dislocations. The critical resolved shear stress was calculated using the equation:

$$\tau_y^\alpha = \eta G b^\alpha \sqrt{\sum_{\beta=1}^{N} \left(K^{\alpha\beta} \rho_d^\beta + L^{\alpha\beta} \rho_{def}^\beta \right)}, \tag{4}$$

where η is a statistical parameter, G is the shear modulus, b^α is the Burgers' vector in the slip plane, $K^{\alpha\beta}$ and $L^{\alpha\beta}$ are the interaction matrices, ρ_d^β and ρ_{def}^β are the densities of dislocations and defects, respectively. Similar equations were used in most of the subsequent crystal plasticity studies, cited below. However, when it comes to coupling the dislocation and defect terms, sometimes the sum of square roots (linear superposition) was used instead of the square root of sums. The issue of choosing the right superposition rule was thoroughly discussed in [18,32]. Also, the latent hardening introduced by means of interaction matrices was sometimes neglected. Similar model was introduced in [54] to study the behaviour of irradiated BCC molybdenum. The novelty of the paper was the utilization of CRSS composed of two terms, namely the thermal and athermal one. Nevertheless, the plastic response was driven by the power law similar to Eq. 2 in the same fashion as in [19].

A model for irradiated austenitic stainless steel was introduced in [55,56]. The hardening law of the crystal plasticity model was enriched by incorporating the effects connected with the emergence of Frank loops and dislocation unlock. The main conceptual difference of this model wrt. to other approaches stems from the fact that instead of supplying the initial defect densities (measured or calculated in lower scale models), different set of material parameters is needed for each level of dpa The model was originally implemented in ZéBuLoN and Cast3M finite element method programs. In [57] its implementation into the more commonly used ABAQUS FEM software was described in detail. Also the validation on simplified microstructures was presented. In [58], the parameter calibration was done and the necessary number of grains and finite elements per grain were investigated. The model developed in the cited papers was then applied in [59] to evaluate the influence of irradiation on the intergranular stress corrosion cracking (IGSCC). The latter phenomenon was observed both in boiling water reactors (BWRs) and pressurized water reactors (PWRs). The developed model was also applied in [60] to study the effect of irradiation up to 13 dpa on the growth and coalescence of voids in FCC single crystals. The authors carried out the crystal plasticity finite element method (CPFEM) simulations of single crystals with voids whose size corresponded to secondary voids resulting from high irradiation levels. The results of simulations enabled to conclude that in materials subjected to irradiation the voids grow faster and coalesce earlier because of more significant plastic slip localization. The irradiated material tends to suffer from macroscopic embrittlement even though fine dimples at the failure site characteristic for ductile failure can be observed. This seemingly paradoxical behaviour can be well explained using the authors' conclusions. El Shawish et al. [3] applied the developed model to investigate the tensile response of the austenitic stainless steel SA304L irradiated to 0.8 dpa. The model of [55] was also used as a benchmark for validating the analytical model of neutron-irradiated austenitic steel in [61]. In addition, the crystal plasticity model implementation using the fast Fourier transforms (FFT) in the CraFT software was presented there. The results of CP simulations were compared against the experimental data from Russian austenitic steels irradiated in fast reactors.

The very detailed crystal plasticity constitutive model of irradiated BCC material was presented in [20]. The model accounts for number density and mean size of the dislocation loops. However, for simplicity only interstitial loops are taken into account, since the vacancy loops are smaller and they do not impede the glide of dislocations considerably. The mobile and immobile dislocation densities were tracked separately on each of 48 slip systems. Various physical phenomena were separately included in the evolution laws. The evolution of the concentrations of irradiation-induced point defects (separately for interstitials and vacancies) is also taken into account. The authors proposed also the phenomenological rule for a rate of annihilation of immobile dislocations and

interstitial loops. The rate of shearing on a given system includes both glide and climb components. This is due to the assumption that dislocation climb enables to overcome barriers to dislocation glide. The model was applied to study the behaviour of modified 9Cr-1Mo ferritic/martensitic steel. Using the model it was possible to simulate both quasistatic and creep tests in the finite element software. The parameters were fitted to experimental data, however no quantitative validation of other predictions was presented. The density and mean size of the loops were assumed to directly depend on the amount of dpa. The model developed in [20] was then used to simulate the plastic flow localization leading to emergence of defect-free channels [62]. The influences of different parameters related to the constitutive model or microstructure idealization used on the shape and width of the channels, as well as defect densities inside them were thoroughly studied. The model was then extended to account for inelastic deformation-driven void nucleation and growth [26]. This way it was possible to study the initiation of failure in irradiated BCC Mod 9Cr-1Mo steel. It is important to note that as this material is characterized by high swelling resistance any possible irradiation-induced voids were neglected. Contary to previous papers, 24 slip systems were considered due to computational limitations.

In [63] the dislocation density based crystal plasticity model accounting for both the network dislocation density and dislocation loop density was reported. Using the model, it was possible to reproduce the softening behaviour observed in irradiated BCC metal subjected to tensile loading. Despite dealing with the BCC material, standard crystal plasticity power law (cf. Eq. 2) was used. The important novelty of this paper was accounting for the dislocation-defect interactions in a tensorial, rather than scalar, fashion. This way, no interaction between the DLs and dislocations lying in parallel planes was introduced. Chakraborty et al. [23] implemented the models presented in [62] and [63], while extending the latter to account for different dislocation densities evolution on different slip systems. In addition, two different integration algorithms were implemented and compared. The effects of different model parameters on the results were discussed. The results were compared against the experimental data and dislocation dynamics simulations available in the literature. In [4], the model accounting for interactions of dislocations with self-interstitial-atom loops, vacancies and copper clusters was used to study changes in mechanical behaviour of pure iron and iron-copper alloys subjected to neutron irradiation. The simulations were compared against dislocation dynamics simulations and experimental data. However, a different set of model parameters had to be used in order to match both types of results.

The crystal plasticity model accounting for irradiation-induced changes was also developed by Xiao et al. In [64] the model for FCC single crystal was presented. One of its crucial aspects is accounting for dislocation-defect interaction in a tensorial fashion. To this aim, the equations developed in [63] enahanced by adding the annihilation probability term developed in [19] were applied. This was done in order to account for a different nature of the most important defects. Barton et al. dealt with irradiated BCC material where the dislocation loops are common. In the case of FCC copper, the SFTs are the major irradiation-induced defects. Since they are 3D objects, their interaction with dislocations is probably different than in the case of DLs. The evolution of dislocation density on each slip system has just two terms accounting for storage and dynamic recovery. In [65] the model was further enhanced by accounting for temperature and implemented in the elastic-viscoplastic self-consistent (EVPSC) model. Using the self-consistent model based on [66] enabled to model the response of a polycrystalline material. The model was then adopted to study the behaviour of BCC iron [67], BCC steel [68] and Fe-Cr alloys [22]. In the first model no conceptual changes were made apart from neglecting the annihilation probability term and accounting for the Hall-Petch hardening. The third one additionaly accounted for the effects of SRCs, Cr solute and lattice resistance friction. In spite of modelling the BCC materials, in both [67] and [22] the standard crystal plasticity power law (Eq. 2) was used in contrast to Kocks-type thermal activation equation (Eq. 3). The latter one was however used in [68].

Another DDCP model was reported in [69]. The dislocation density based crystal plasticity hardening model shares common concepts with the paper of [20], although some ot the effects (concentrations of point defects, cross slip and climb terms in evolution equations for dislocation densities, annihilation of immobile dislocation due to interaction with loops) are disregarded. The novelty of the model lies in including damage. The model was applied to simulate the behaviour of body centered cubic ferritic A508-3 steel which is used to build reactor pressure vessels in China. Similar model for FCC metals was presented in [70]. However, contrary to [69], where the mobile and immobile dislocation densities were tracked separately, here edge and screw dislocation populations are divided. Since the SFTs are basic irradiation-induced defects in FCC metals, the defect evolution model based on [19] was applied.

The model for FCC austenitic stainless steels was presented in [71]. The contributions to CRSS arising from dislocation forest, DLs and SRCs are combined using the quadratic sum. On the other hand, the friction due to solid solution and Hall-Petch effect are included by linear superposition. Dislocation population evolves separately on each slip system, while the DLs and SRCs are assumed to be uniformly distributed. The polycrystalline behaviour was obtained by implementing the model in the elasto-plastic self-consistent model of Berveiller and Zaoui (BZ) [72]. Additionally, the analytical model for yield stress prediction was presented. The authors adjusted the set of parameters to obtain the stress strain curve of the unirradiated material. The response of the irradiated material was simulated to be in reasonable agreement with experimental data by proper selection of DL density and a parameter accounting for annihilation of radiation defects by moving dislocations. The effect of SRCs was disregarded at the validation stage.

Somewhat more complicated model was presented in [73]. Since the model was build for RPV steels, the plastic slip rate was a harmonic sum of the slip rates controlled by the jog-drag and lattice friction. While the classical power law was used for the jog-drag term, the thermal activation law was used for the lattice friction regime. Note however, that the classical Kocks law (Eq. 3) was modified by using the square root instead of two exponents. Similarly as in [71], the defects considered were DLs and SRCs. Interestingly, three homogenization schemes were applied, namely the SC BZ, the CPFEM and FFT approaches. Strangely, the authors compared the results obtained using the small strain (BZ) and finite strain (FFT) formulations in the finite strain regime where the small strain assumption is invalid. Contrary to other papers (e. g. [74]), the yield stress being higher than subsequent flow stress is believed to be a result of static aging rather than softening related to creation of defect-free channels. Another issue is the result that at low temperature there is no irradiation hardening – this is however only the prediction that was not confirmed by any experimental data so far.

A model for BCC material conceptually similar to [73] was developed in [75]. The slip rate is calculated as a harmonic sum of thermal and athermal terms. Both terms were calculated using the thermally activated Kocks-type law (cf. Eq. 3). The thermal term depends on an average length of screw dislocation segment, and the athermal one on the distance swept by a kink pair before its annihilation with another kink pair. The results were used as an input to probabilistic assessment of brittle fracture using the Weibull distribution.

4. Nanoindentation

In the papers cited herein, the polycrystalline response was obtained either by using the self-consistent (SC) [22,41,42,65,67,68,71,73], the FEM [3,11,20,23,43,45,57–60,62,63,69,70,75] or FFT based ([3,44,61,71]) homogenization techniques. In the self-consistent model, each grain is treated as an uniformly deforming ellipsoidal inclusion [49,76]. Although such simplification leads to numerically very efficient formulation, the complex geometry on the single or polycrystal level, grain neighbouring effects and intragrain phenomena cannot be studied using such an approach. On the other hand, the CPFEM is very flexible in addressing such issues, but increasing number of grains and fine mesh leads to quick
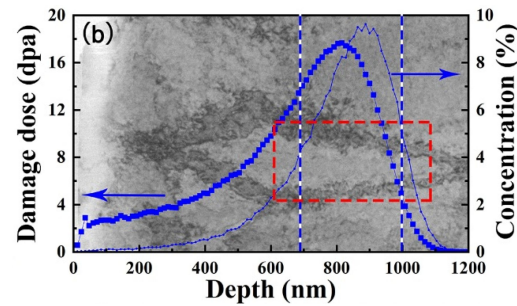
Figure 5. Image showing the damage profile of tungsten implanted with He ions simulated with SRIM software superimposed on TEM image [83].
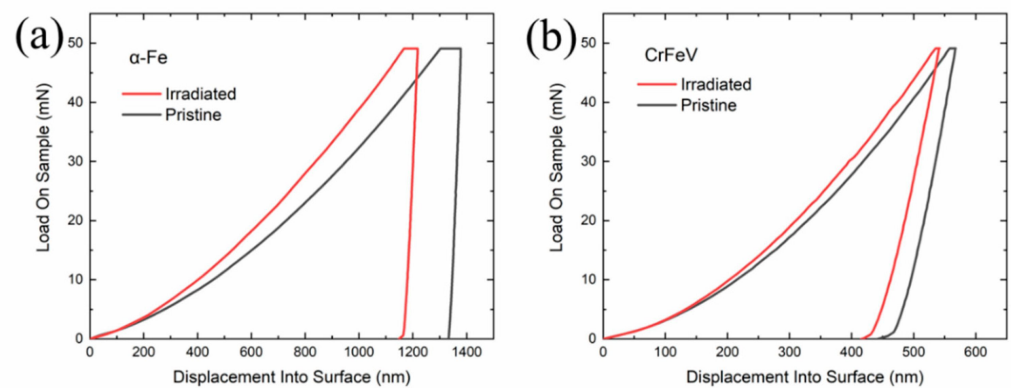

Figure 6. Illustration of the influence of irradiation on instrumented indentation data. Load-displacement curves: a) α-Fe, b) CrFeV alloy [84].

increase of the computational cost. Finally the FFT-based approach joins some assets of the SC approach (numerical efficiency) with others of the CPFEM (explicitly addressing the microstructure of the material). However, it also requires the domain and boundary conditions to be periodic and thus similarly to the SC method is not suitable to study complex geometry or boundary conditions.

Constitutive models of irradiated materials should be always validated against the experimental data. However, testing the material specimen in reactor conditions is difficult from the practical perspective. First, the specimen has to be subjected to neutron radiation for a long time in order to achieve desired level of dpa. Second, the specimen irradiated with neutrons is active and has to be tested inside hot cells. On the other hand, high levels of irradiation can be achieved by irradiating the material for much shorter times using ions or protons. Since ions do not cause fission, transmutation or excitation, the materials irradiated (or, in other words, implanted) with ions can be also tested in standard mechanical laboratories.

However, in contrast to neutrons, ions are charged and thus they can penetrate the material to a very shallow depths only, cf. Fig. 5. Since the thin surface of a material cannot be mechanically tested using conventional mechanical testing, typically the instrumented (nano)indentation test (cf. e. g. [39,40,77–82]) is used in order to obtain the properties of the irradiated layer. As it was already mentioned in this review, the basic mechanistic effect of irradiation is irradiation hardening. In terms of load-penetration curves this is visible by means of higher load value at the same displacement in the case of ion implanted material, cf. Fig. 6.

So far, there is no simple and reliable theory to link the indentation load-penetration curve to elastic and plastic properties of the material. Thus, since nanoindentation test is generally performed on one grain of the polycrystalline material, the crystal plasticity finite element method can be successfully used to obtain the material properties from such a test [50,85–90]. In [91] the crystal plasticity model with Voce hardening was applied to
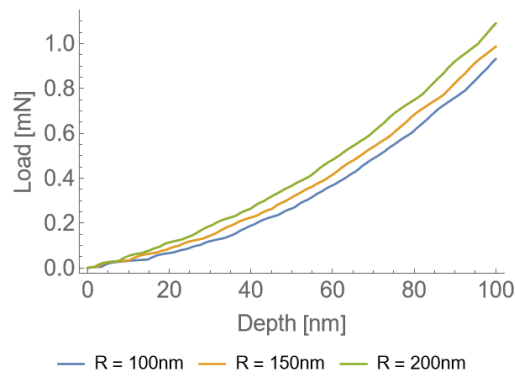
Figure 7. Load-displacement curves obtained for different radii of the Berkovich tip.

simulate the indentation of pure Zr in virgin and irradiated state. The modified plastic properties of the irradiated material were simply obtained by changing the value of the initial CRSS of each slip system only, rather than by modification of the model itself. In [92] the strain-gradient crystal plasticity model was adopted to model the behaviour of ion-irradiated FCC single crystals. The irradiation effect was taken into account by adding the irradiation-induced defects term to the CRSS. The defect density was specified non-uniformly along the sample's thickness. In [93] the DDCP model similar to [69] was applied in order to study the irradiation effect on hardness of Chinese RPV A508-3 steel.

The behaviour of self-ion irradiated tungsten was studied in [9] using nanoindentation, high-resolution EBSD and small-strain strain-gradient crystal plasticity. To account for irradiation effect, the additional term τ_H was added to the CRSS. This term depended on the density of dislocation loops measured in TEM. Moreover, this term was decreasing with strain which accounted for weakening of defects by gliding dislocations – thus a strain softening model was used. The CPFEM simulations of indentation in tungsten were also reported in [94]. The model includes the irradiation hardening terms coming from voids and loops. However, only hardness values were compared against the experimental data and no load-displacement curves were provided.

An interesting model able to capture both irradiation effects and pop-in behaviour in tungsten was published in [95]. The possibility to pop-in was taken into account by introducing the probabilistic pop-in stress. The CRSS included the terms related to DLs, He bubbles, SSDs, GNDs and lattice friction. The model correctly predicted that irradiation leads to inhibiting the pop-in possibility.

While modelling indentation of ion-implanted materials using CPFEM one should be aware of several important effects. First, ideally the plastic zone should not exceed the flat part of dpa before the peak (cf. Fig. 5). Since the plastic zone is 5-10 times larger than the indenter penetration, this results in severe restriction on the maximum penetration depth or necessitates usage of high ion energies (that lead to considerable ion penetration). Alternatively, one can consider variable defect density as it was done in [92]. Performing nanoindentation at very small depth poses further challenges. First, at small depths the size effect plays important role and one should use a size-sensitive model, e. g. [89,96–98]. Second, in the case of using pyramidal indenters, the influence of tip bluntness considerably affects the obtained mechanical response [99–103], thus necessitating to explicitly account for it. The simulated load-displacement curves using Berkovich indenter blunted with three parabolic cylinders with different values of tip radius R (details of the CPFEM simulation can be found in [104]) are shown in Fig. 7. One can see that the influence of tip radius is considerable. On the other hand, the influence of friction on the load-displacement curves can be neglected for small depths (cf. Fig. 12 in [90]).

5. Conclusions

Based on the conducted literature review one can conclude that:

- Massive construction of new nuclear power plants is an essential requirement for meeting the CO_2 reduction goals [1].
- Accounting for the effect of irradiation on mechanical properties in crystal plasticity theory started about 15 years ago and is still an area of active research.
- In particular, there is no consensus among different authors on whether various contributions to the CRSS should be superposed linearly or quadratically.
- Ion implantation is a cheap alternative to neutron irradiation but in order to measure the change in mechanical properties due to ion irradaition instrumented nanoindentation testing combined with CPFEM modelling is indispensable.
- One should account for ion penetration depth, size effects and indenter tip imperfection while performing CPFEM simulations of nanoindentation.

Data Availability Statement: No new data were created or analyzed in this study.

Conflicts of Interest: The authors declare no conflict of interest.

Abbreviations

The following abbreviations are used in this manuscript:

NPP	nuclear power plant
PWR	pressurized water reactor
HCP	hexagonal close packed
ASS	austenitic stainless steels
FCC	face centered cubic
RPV	reactor pressure vessel
BCC	body centered cubic
DBTT	ductile to brittle transition temperature
Gen-IV	generation IV
GIF	Generation-IV International Forum
VHTR	very high temperature gas-cooled reactor
GFR	gas-cooled fast reactor
SFR	sodium-cooled fast reactor
LFR	lead-cooled fast reactor
MSR	molten salt reactor
SCWR	super-critical water-cooled reactor
FM	ferritic-martensitic
ODS	oxide dispersion strenghtened
PKA	primary knock-on atom
SFT	stacking fault tetrahedron
DL	dislocation loop
SRC	solute rich cluster
DBH	dispersed barrier hardening
dpa	displacement per atom
PCP	phenomenological crystal plasticity
DDCP	dislocation density based crystal plasticity
CRSS	critical resolved shear stress
RSS	resolved shear stress
IGSCC	intergranular stress corrosion cracking
CPFEM	crystal plasticity finite element method
FFT	fast Fourier transform
EVPSC	elastic-viscoplastic self-consistent
BZ	Berveiller and Zaoui
SC	self-consistent

References

1. Goldstein, J.; Qvist, S. *A bright future: How some countries have solved climate change and the rest can follow*; PublicAffairs, 2019.
2. Fernández-Arias, P.; Vergara, D.; Orosa, J.A. A Global Review of PWR Nuclear Power Plants. *Applied Sciences* **2020**, *10*. https://doi.org/10.3390/app10134434.
3. El Shawish, S.; Vincent, P.G.; Moulinec, H.; Cizelj, L.; Gélébart, L. Full-field polycrystal plasticity simulations of neutron-irradiated austenitic stainless steel: A comparison between FE and FFT-based approaches. *J. Nucl. Mater.* **2020**, *529*, 151927.
4. Chakraborty, P.; Biner, S.B. Crystal plasticity modeling of irradiation effects on flow stress in pure-iron and iron-copper alloys. *Mechanics of Materials* **2016**, *101*, 71–80.
5. Murty, K.L.; Charit, I. Structural materials for Gen-IV nuclear reactors: Challenges and opportunities. *J. Nucl. Mater.* **2008**, *383*, 189–195.
6. Abram, T.; Ion, S. Generation-IV nuclear power: A review of the state of the science. *Energy Policy* **2008**, *36*, 4323–4330.
7. Yvon, P.; Le Flem, M.; Cabet, C.; Seran, J.L. Structural materials for next generation nuclear systems: Challenges and the path forward. *Nucl. Eng. Des.* **2015**, *294*, 161–169.
8. Frelek-Kozak, M.; Kurpaska, .; Mulewska, K.; Zieliński, M.; Diduszko, R.; Kosińska, A.; Kalita, D.; Chromiński, W.; Turek, M.; Kaszyca, K.; et al. Mechanical behavior of ion-irradiated ODS RAF steels strengthened with different types of refractory oxides. *Applied Surface Science* **2023**, *610*, 155465. https://doi.org/https://doi.org/10.1016/j.apsusc.2022.155465.
9. Das, S.; Yu, H.; Mizohata, K.; Tarleton, E.; Hofmann, F. Modified deformation behaviour of self-ion irradiated tungsten: a combined nano-indentation, HR-EBSD and crystal plasticity study. *International Journal of Plasticity* **2020**, *135*, 102817.
10. El-Atwani, O.; Li, N.; Li, M.; Devaraj, A.; Baldwin, J.; Schneider, M.; Sobieraj, D.; Wróbel, J.; Nguyen-Manh, D.; Maloy, S.; et al. Outstanding radiation resistance of tungsten-based high-entropy alloys. *Science advances* **2019**, *5*, eaav2002.
11. Wang, Y.; Sun, X.; Zhao, J. A mechanism-based quantitative multi-scale framework for investigating irradiation hardening of tungsten at low temperature. *Mater. Sci. Eng. A* **2020**, *774*, 138941.
12. Garner, F.; Hamilton, M.; Panayotou, N.; Johnson, G. The microstructural origins of yield strength changes in AISI 316 during fission or fusion irradiation. *Journal of Nuclear Materials* **1981**, *104*, 803–807.
13. Odette, G.; Lucas, G. Recent progress in understanding reactor pressure vessel steel embrittlement. *Radiation effects and defects in solids* **1998**, *144*, 189–231.
14. Zinkle, S.; Maziasz, P.; Stoller, R. Dose dependence of the microstructural evolution in neutron-irradiated austenitic stainless steel. *Journal of Nuclear materials* **1993**, *206*, 266–286.
15. Zhang, H.; Long, B.; Dai, Y. Metallography studies and hardness measurements on ferritic/martensitic steels irradiated in STIP. *Journal of Nuclear Materials* **2008**, *377*, 122–131. Spallation Materials Technology, https://doi.org/https://doi.org/10.1016/j.jnucmat.2008.02.037.
16. English, C.; Hyde, J. Radiation damage of reactor pressure vessel steels **2012**.
17. Slugeň, V.; Sojak, S.; Egger, W.; Krsjak, V.; Simeg Veternikova, J.; Petriska, M. Radiation damage of reactor pressure vessel steels studied by positron annihilation spectroscopy—A Review. *Metals* **2020**, *10*, 1378.
18. Monnet, G. Multiscale modeling of irradiation hardening: Application to important nuclear materials. *J. Nucl. Mater.* **2018**, *508*, 609–627.
19. Krishna, S.; Zamiri, A.; De, S. Dislocation and defect density-based micromechanical modeling of the mechanical behavior of FCC metals under neutron irradiation. *Philos. Mag.* **2010**, *90*, 4013–4025.
20. Patra, A.; McDowell, D. Crystal plasticity-based constitutive modelling of irradiated BCC structures. *Philos. Mag.* **2012**, *92*, 861–887.
21. Patra, A.; Tomé, C.; Golubov, S. Crystal plasticity modeling of irradiation growth in Zircaloy-2. *Philos. Mag.* **2017**, *97*, 2018–2051.
22. Xiao, X.; Terentyev, D.; Yu, L.; Bakaev, A.; Jin, Z.; Duan, H. Investigation of the thermo-mechanical behavior of neutron-irradiated Fe-Cr alloys by self-consistent plasticity theory. *J. Nucl. Mater.* **2016**, *477*, 123–133.
23. Chakraborty, P.; Biner, S.; Zhang, Y.; Spencer, B. Crystal plasticity model of reactor pressure vessel embrittlement in Grizzly. Technical report, Idaho National Lab.(INL), Idaho Falls, ID (United States), 2015.

24. Seeger, A. On the theory of radiation damage and radiation hardening. In Proceedings of the Proceedings of the 2nd UN International Conference on Peaceful Uses of Atomic Energy, 1958, Vol. 6, p. 250.

25. Roldán, M.; Sánchez, F.J.; Fernández, P.; Ortiz, C.J.; Gómez-Herrero, A.; Rey, D.J. Dislocation Loop Generation Differences between Thin Films and Bulk in EFDA Pure Iron under Self-Ion Irradiation at 20 MeV. *Metals* **2021**, *11*. https://doi.org/10.3390/met11122000.

26. Patra, A.; McDowell, D. A void nucleation and growth based damage framework to model failure initiation ahead of a sharp notch in irradiated BCC materials. *J. Mech. Phys. Solids* **2015**, *74*, 111–135.

27. Weeks, J.; Czajkowski, C.; Tichler, P. Effects of high thermal and high fast fluences on the mechanical properties of type 6061 aluminum on the HFBR. In Proceedings of the Effects of Radiation on Materials: 14th International Symposium (Volume II). ASTM International, 1990.

28. Griffiths, M. Effect of Neutron Irradiation on the Mechanical Properties, Swelling and Creep of Austenitic Stainless Steels. *Materials* **2021**, *14*. https://doi.org/10.3390/ma14102622.

29. Bergner, F.; Hernández-Mayoral, M.; Heintze, C.; Konstantinović, M.J.; Malerba, L.; Pareige, C. TEM Observation of Loops Decorating Dislocations and Resulting Source Hardening of Neutron-Irradiated Fe-Cr Alloys. *Metals* **2020**, *10*. https://doi.org/10.3390/met10010147.

30. Zhang, F.; Boatner, L.; Zhang, Y.; Chen, D.; Wang, Y.; Wang, L. Swelling and Helium Bubble Morphology in a Cryogenically Treated FeCrNi Alloy with Martensitic Transformation and Reversion after Helium Implantation. *Materials* **2019**, *12*. https://doi.org/10.3390/ma12172821.

31. Kinchin, G.H.; Pease, R.S. The displacement of atoms in solids by radiation. *Reports on progress in physics* **1955**, *18*, 1.

32. Was, G.S. *Fundamentals of radiation materials science: metals and alloys*; Springer, 2017.

33. Ziegler, J.F.; Ziegler, M.; Biersack, J. SRIM – The stopping and range of ions in matter (2010). *Nuclear Instruments and Methods in Physics Research Section B: Beam Interactions with Materials and Atoms* **2010**, *268*, 1818–1823. 19th International Conference on Ion Beam Analysis, https://doi.org/https://doi.org/10.1016/j.nimb.2010.02.091.

34. Crocombette, Jean-Paul.; Van Wambeke, Christian. Quick calculation of damage for ion irradiation: implementation in Iradina and comparisons to SRIM. *EPJ Nuclear Sci. Technol.* **2019**, *5*, 7. https://doi.org/10.1051/epjn/2019003.

35. Perzyna, P. Theory of viscoplasticity of irradiated materials. *Archives of Mechanics* **1974**, *26*, 81–93.

36. Arsenlis, A.; Wirth, B.; Rhee, M. Dislocation density-based constitutive model for the mechanical behaviour of irradiated Cu. *Philos. Mag.* **2004**, *84*, 3617–3635.

37. Skoczeń, B.; Ustrzycka, A. Kinetics of evolution of radiation induced micro-damage in ductile materials subjected to time-dependent stresses. *Int. J. Plast.* **2016**, *80*, 86–110.

38. Ryś, M.; Skoczeń, B. Coupled constitutive model of damage affected two-phase continuum. *Mech. Mater.* **2017**, *115*, 1–15.

39. Ustrzycka, A.; Skoczeń, B.; Nowak, M.; Kurpaska, Ł.; Wyszkowska, E.; Jagielski, J. Elastic–plastic-damage model of nano-indentation of the ion-irradiated 6061 aluminium alloy. *Int. J. Damage Mech.* **2020**, p. 1056789520906209.

40. Nowak, M.; Mulewska, K.; Azarov, A.; Ustrzycka, A.; et al. A peridynamic elasto-plastic damage model for ion-irradiated materials. *International Journal of Mechanical Sciences* **2023**, *237*, 107806.

41. Deo, C.; Tomé, C.; Lebensohn, R.; Maloy, S. Modeling and simulation of irradiation hardening in structural ferritic steels for advanced nuclear reactors. *J. Nucl. Mater.* **2008**, *377*, 136–140.

42. Onimus, F.; Béchade, J.L. A polycrystalline modeling of the mechanical behavior of neutron irradiated zirconium alloys. *J. Nucl. Mater.* **2009**, *384*, 163–174.

43. Erinosho, T.; Dunne, F. Strain localization and failure in irradiated zircaloy with crystal plasticity. *Int. J. Plast.* **2015**, *71*, 170–194.

44. Onimus, F.; Gelebart, L.; Brenner, R. Polycrystalline simulations of in-reactor deformation of recrystallized Zircaloy-4 tubes: Fast Fourier Transform computations and mean-field self-consistent model. *International Journal of Plasticity* **2022**, *153*, 103272.

45. Vincent, L.; Libert, M.; Marini, B.; Rey, C. Towards a modelling of RPV steel brittle fracture using crystal plasticity computations on polycrystalline aggregates. *J. Nucl. Mater.* **2010**, *406*, 91–96.

46. Asaro, R.J.; Needleman, A. Texture Development and Strain Hardening in Rate Dependent Polycrystals. *Acta Metall.* **1985**, *33*, 923–953.

47. Frydrych, K.; Kowalczyk-Gajewska, K. A three-scale crystal plasticity model accounting for grain refinement in FCC metals subjected to severe plastic deformations. *Mater. Sci. Eng. A* **2016**, *658*, 490 – 502.

48. Frydrych, K. Simulations of Grain Refinement in Various Steels Using the Three-Scale Crystal Plasticity Model. *Metall. Mater. Trans. A* **2019**, *50*, 4913–4919.

49. Girard, G.; Frydrych, K.; Kowalczyk-Gajewska, K.; Martiny, M.; Mercier, S. Cyclic response of electrodeposited copper films. Experiments versus elastic-viscoplastic mean-field approach predictions. *Mech. Mater.* **2021**, *153*, 1–17.

50. Frydrych, K.; Dominguez, J.; Alava, M.; Papanikolaou, S. Multiscale nanoindentation modeling of concentrated solid solutions: A continuum plasticity model. *Mechanics of Materials* **2023**, *181*, 104644. https://doi.org/https://doi.org/10.1016/j.mechmat.2023.104644.

51. Kothari, M.; Anand, L. Elasto-viscoplastic constitutive equations for polycrystalline metals: Application to tantalum. *J. Mech. Phys. Solids* **1998**, *46*, 51 – 83.

52. Kocks, U.F.; Argon, A.S.; Ashby, M.F. Thermodynamics and kinetics of slip. *Progress in Materials Science* **1975**, *19*.

53. Orowan, E. Problems of plastic gliding. *Proc. Phys. Soc.* **1940**, *52*, 8.

54. Krishna, S.; De, S. A temperature and rate-dependent micromechanical model of molybdenum under neutron irradiation. *Mech. Mater.* **2011**, *43*, 99–110.

55. Han, X. Modeling of cavity swelling-induced embrittlement in irradiated austenitic stainless steels; Modelisation de la fragilisation due au gonflement dans les aciers inoxydables austenitiques irradies. PhD thesis, Ecole Nationale Superieure des Mines de Paris Univ., Paris, France, 2012.

56. Tanguy, B.; Han, X.; Besson, J.; Forest, S.; Robertson, C.; Rupin, N. Dislocations and irradiation defects-based micromechanical modelling for neutron irradiated austenitic stainless steels. In Proceedings of the International Symposium on Plasticity, 2013, pp. 3–8.

57. El Shawish, S.; Cizelj, L.; Tanguy, B.; Han, X.; Hure, J. Extended crystal plasticity finite element approach for neutron irradiated austenitic stainless steels. In Proceedings of the 23rd Int. Conf. Nuclear Energy for New Europe, 2014.

58. El Shawish, S.; Cizelj, L.; Tanguy, B.; Han, X.; Hure, J. Macroscopic Validation of the Micromechanical Model for Neutron-Irradiated Stainless Steel. In Proceedings of the 25th Int. Conf. Nuclear Energy for New Europe, 2016.

59. Hure, J.; El Shawish, S.; Cizelj, L.; Tanguy, B. Intergranular stress distributions in polycrystalline aggregates of irradiated stainless steel. *J. Nucl. Mater.* **2016**, *476*, 231–242.

60. Ling, C.; Tanguy, B.; Besson, J.; Forest, S.; Latourte, F. Void growth and coalescence in triaxial stress fields in irradiated FCC single crystals. *J. Nucl. Mater.* **2017**, *492*, 157–170.

61. Vincent, P.G.; Moulinec, H.; Joëssel, L.; Idiart, M.I.; Gărăjeu, M. Porous polycrystal plasticity modeling of neutron-irradiated austenitic stainless steels. *J. Nucl. Mater.* **2020**, p. 152463.

62. Patra, A.; McDowell, D. Continuum modeling of localized deformation in irradiated BCC materials. *J. Nucl. Mater.* **2013**, *432*, 414–427.

63. Barton, N.; Arsenlis, A.; Marian, J. A polycrystal plasticity model of strain localization in irradiated iron. *J. Mech. Phys. Solids* **2013**, *61*, 341–351.

64. Xiao, X.; Song, D.; Xue, J.; Chu, H.; Duan, H. A size-dependent tensorial plasticity model for FCC single crystal with irradiation. *Int. J. Plast.* **2015**, *65*, 152–167.

65. Xiao, X.; Song, D.; Xue, J.; Chu, H.; Duan, H. A self-consistent plasticity theory for modeling the thermo-mechanical properties of irradiated FCC metallic polycrystals. *J. Mech. Phys. Solids* **2015**, *78*, 1–16.

66. Sabar, H.; Berveiller, M.; Favier, V.; Berbenni, S. A new class of micro-micro models for elastic-viscoplastic heterogeneous materials. *Int. J. Solids Struct.* **2002**, *39*, 3257–3276.

67. Xiao, X.; Terentyev, D.; Yu, L.; Song, D.; Bakaev, A.; Duan, H. Modelling irradiation-induced softening in BCC iron by crystal plasticity approach. *J. Nucl. Mater.* **2015**, *466*, 312–315.

68. Song, D.; Xiao, X.; Xue, J.; Chu, H.; Duan, H. Mechanical properties of irradiated multi-phase polycrystalline BCC materials. *Acta Mechanica Sinica* **2015**, *31*, 191–204.

69. Nie, J.; Liu, Y.; Xie, Q.; Liu, Z. Study on the irradiation effect of mechanical properties of RPV steels using crystal plasticity model. *Nucl. Eng. Technol.* **2019**, *51*, 501–509.

70. Nie, J.; Liu, Y.; Lin, P.; Xie, Q.; Liu, Z. A crystal plasticity model with irradiation effect for the mechanical behavior of FCC metals. *Acta Mechanica Solida Sinica* **2019**, *32*, 675–687.

71. Monnet, G.; Mai, C. Prediction of irradiation hardening in austenitic stainless steels: Analytical and crystal plasticity studies. *J. Nucl. Mater.* **2019**, *518*, 316–325.

72. Berveiller, M.; Zaoui, A. An extension of the self-consistent scheme to the plastically flowing polycrystals. *J. Mech. Phys. Solids* **1978**, *26*, 325–344.

73. Monnet, G.; Vincent, L.; Gélébart, L. Multiscale modeling of crystal plasticity in Reactor Pressure Vessel steels: Prediction of irradiation hardening. *J. Nucl. Mater.* **2019**, *514*, 128–138.

74. Patra, A.; McDowell, D. Crystal plasticity investigation of the microstructural factors influencing dislocation channeling in a model irradiated BCC material. *Acta Mater.* **2016**, *110*, 364–376.

75. Singh, K.; Robertson, C.; Bhaduri, A. Brittle fracture model parameter estimation for irradiated BCC material through dislocation based crystal plasticity model. *Frat. ed Integrità Strutt.* **2019**, *13*, 319–330.

76. Lebensohn, R.A.; Tomé, C.N. A self-consistent anisotropic approach for the simulation of plastic deformation and texture development of polycrystals: Application to zirconium alloys. *Acta Metall. Mater.* **1993**, *41*, 2611–2624.

77. Hosemann, P.; Vieh, C.; Greco, R.; Kabra, S.; Valdez, J.; Cappiello, M.; Maloy, S. Nanoindentation on ion irradiated steels. *J. Nucl. Mater.* **2009**, *389*, 239–247.

78. Hosemann, P.; Kiener, D.; Wang, Y.; Maloy, S.A. Issues to consider using nano indentation on shallow ion beam irradiated materials. *J. Nucl. Mater.* **2012**, *425*, 136–139.

79. Kucharski, S.; Jarząbek, D. Depth dependence of nanoindentation pile-up patterns in copper single crystals. *Metall. Mater. Trans. A* **2014**, *45*, 4997–5008.

80. Zaborowska, A.; Kurpaska, .; Wyszkowska, E.; Clozel, M.; Vanazzi, M.; Di Fonzo, F.; Turek, M.; Jóźwik, I.; Kosińska, A.; Jagielski, J. Influence of ion irradiation on the nanomechanical properties of thin alumina coatings deposited on 316L SS by PLD. *Surface and Coatings Technology* **2020**, *386*, 125491. https://doi.org/https://doi.org/10.1016/j.surfcoat.2020.125491.

81. Clozel, M.; Kurpaska, L.; Jóźwik, I.; Jagielski, J.; Turek, M.; Diduszko, R.; Wyszkowska, E. Nanomechanical properties of low-energy Fe-ion implanted Eurofer97 and pure Fe. *Surface and Coatings Technology* **2020**, *393*, 125833. https://doi.org/https://doi.org/10.1016/j.surfcoat.2020.125833.

82. Mulewska, K.; Rovaris, F.; Dominguez-Gutierrez, F.; Huo, W.; Kalita, D.; Jozwik, I.; Papanikolaou, S.; Alava, M.; Kurpaska, L.; Jagielski, J. Self-ion irradiation effects on nanoindentation-induced plasticity of crystalline iron: A joint experimental and computational study. *Nuclear Instruments and Methods in Physics Research Section B: Beam Interactions with Materials and Atoms* **2023**, *539*, 55–61. https://doi.org/https://doi.org/10.1016/j.nimb.2023.03.004.

83. Huang, W.; Sun, M.; Wen, W.; Yang, J.; Xie, Z.; Liu, R.; Wang, X.; Wu, X.; Fang, Q.; Liu, C. Strain Profile in the Subsurface of He-Ion-Irradiated Tungsten Accessed by S-GIXRD. *Crystals* **2022**, *12*. https://doi.org/10.3390/cryst12050691.

84. Su, Y.; Xia, S.; Huang, J.; Liu, Q.; Liu, H.; Wang, C.; Wang, Y. Irradiation Behaviors in BCC Multi-Component Alloys with Different Lattice Distortions. *Metals* **2021**, *11*. https://doi.org/10.3390/met11050706.

85. Kucharski, S.; Stupkiewicz, S.; Petryk, H. Surface Pile-Up Patterns in Indentation Testing of Cu Single Crystals. *Exper. Mech.* **2014**, *54*, 957–969.

86. Petryk, H.; Stupkiewicz, S.; Kucharski, S. On direct estimation of hardening exponent in crystal plasticity from the spherical indentation test. *Int. J. Solids Struct.* **2017**, *112*, 209–221.

87. Chakraborty, A.; Eisenlohr, P. Evaluation of an inverse methodology for estimating constitutive parameters in face-centered cubic materials from single crystal indentations. *European Journal of Mechanics - A/Solids* **2017**, *66*, 114–124. https://doi.org/https://doi.org/10.1016/j.euromechsol.2017.06.012.

88. Frydrych, K. Crystal plasticity finite element simulations of the indentation test. *Comput. Methods Mater. Sci.* **2019**, *19*, 41–49.

89. Ryś, M.; Stupkiewicz, S.; Petryk, H. Micropolar regularization of crystal plasticity with the gradient-enhanced incremental hardening law. *Int. J. Plast.* **2022**.

90. Frydrych, K.; Papanikolaou, S. Unambiguous Identification of Crystal Plasticity Parameters from Spherical Indentation. *Crystals* **2022**, *12*, 1341.

91. Wang, Q.; Cochrane, C.; Skippon, T.; Wang, Z.; Abdolvand, H.; Daymond, M.R. Orientation-dependent irradiation hardening in pure Zr studied by nanoindentation, electron microscopies, and crystal plasticity finite element modeling. *Int. J. Plast.* **2019**, *124*, 133 – 154.

92. Xiao, X.; Chen, L.; Yu, L.; Duan, H. Modelling nano-indentation of ion-irradiated FCC single crystals by strain-gradient crystal plasticity theory. *Int. J. Plast.* **2019**, *116*, 216–231.

93. Nie, J.; Lin, P.; Liu, Y.; Zhang, H.; Wang, X. Simulation of the irradiation effect on hardness of Chinese HTGR A508-3 steels with CPFEM. *Nucl. Eng. Technol.* **2019**, *51*, 1970–1977.

94. Shi, J.; Liu, G.; Wu, K.; Yu, P.; Zhu, H.; Zhao, G.; Shen, Y. Experiments and/or crystal plasticity finite element modeling of the mechanical properties of pristine and irradiated tungsten single crystal. *International Journal of Plasticity* **2022**, *154*, 103293.

95. Xiao, X.; Li, S.; Yu, L. Effect of irradiation damage and indenter radius on pop-in and indentation stress-strain relations: Crystal plasticity finite element simulation. *Int. J. Mech. Sci.* **2021**, *199*, 106430.

96. Petryk, H.; Stupkiewicz, S. A minimal gradient-enhancement of the classical continuum theory of crystal plasticity. Part I: The hardening law. *Arch. Mech.* **2016**, *68*, 459–485.

97. Stupkiewicz, S.; Petryk, H. A minimal gradient-enhancement of the classical continuum theory of crystal plasticity. Part II: Size effects. *Arch. Mech.* **2016**, *68*, 487–513.

98. Lewandowski, M.; Stupkiewicz, S. Size effects in wedge indentation predicted by a gradient-enhanced crystal-plasticity model. *Int. J. Plast.* **2018**.

99. Torres-Torres, D.; Muñoz-Saldaña, J.; Gutierrez-Ladron-de Guevara, L.; Hurtado-Macías, A.; Swain, M. Geometry and bluntness tip effects on elastic–plastic behaviour during nanoindentation of fused silica: experimental and FE simulation. *Model. Simul. Mater. Sci. Eng.* **2010**, *18*, 075006.

100. Krier, J.; Breuils, J.; Jacomine, L.; Pelletier, H. Introduction of the real tip defect of Berkovich indenter to reproduce with FEM nanoindentation test at shallow penetration depth. *J. Mater. Res.* **2012**, *27*, 28–38.

101. Čech, J.; Haušild, P.; Kovářík, O.; Materna, A. Examination of Berkovich indenter tip bluntness. *Materials & Design* **2016**, *109*, 347–353.

102. Kovář, J.; Fuis, V.; Tomáštík, J. Influencing the indentation curves by the bluntness of the Berkovich indenter at the FEM modelling **2020**.

103. Sanchez-Camargo, C.M.; Hor, A.; Mabru, C. A robust inverse analysis method for elastoplastic behavior identification using the true geometry modeling of Berkovich indenter. *Int. J. Mech. Sci.* **2020**, *171*, 105370.

104. Frydrych, K. The influence of the Berkovich tip defect on the results of the nanoindentation simulations. *In preparation* **2023**.